Experimental and theoretical investigation of the dry ice sublimation temperature for varying far-field pressure and CO_2 concentration

A.S. Purandare [*], W.M. Verbruggen, S. Vanapalli [*]

Applied Thermal Sciences Laboratory, Faculty of Science and Technology, University of Twente, Post Bus 217, 7500 AE Enschede, the Netherlands

ARTICLE INFO

ABSTRACT

Solid carbon dioxide, also known as dry ice, is extensively used in various applications, such as cleaning large telescopes, refrigeration, spray cooling, and biological processes like cryopreservation. In standard atmospheric conditions, dry ice sublimates continuously because the triple point pressure of carbon dioxide is higher than the atmospheric pressure. While the sublimation temperature of dry ice at atmospheric pressure is widely reported in the literature to be approximately -78.5 °C, this value is only conditionally true as it refers to dry ice exposed to an ambient saturated with its vapor. In reality, dry ice is mainly utilized in an unsaturated atmosphere. This study investigates the effect of the atmosphere on the sublimation temperature of a dry ice sphere, both experimentally and theoretically. Specifically, the far-field pressure is varied from 0.6 bar to 1.3 bar in steps of 0.1 bar, and the far-field CO_2 concentration is varied from 100%vol to 0%vol in steps of 20%vol. The results show that the sublimation temperature reduces and reaches a lower thermodynamic wet-bulb temperature when the far-field CO_2 concentration is lowered from the previously set value at a given ambient pressure. The lowest value of the sublimation temperature, for the ambient pressure of 1 atm and 0%vol CO_2 concentration, is measured to be -97.3 °C, which deviates from the commonly quoted value in the literature by approximately 19 °C. Finally, the results are presented in the form of an extended phase diagram showing the solid-vapor coexistence line for various far-field CO_2 concentrations in comparison to the standard coexistence line present on the phase diagram. A mathematical model that considers heat and mass transport phenomena in the surroundings of a dry ice sphere is developed, and its predictions are found to be in encouraging agreement with the experimental results. This study provides important insights into the behavior of dry ice under different atmospheric conditions and can be useful in various industrial and scientific applications.

1. Introduction

The triple point pressure of carbon dioxide lies above ambient pressure preventing liquid phase and causing only the solid and gaseous phase to exist at normal atmospheric conditions. The solid form of carbon dioxide, popularly known as dry ice, permanently sublimates at -78.5 °C in a surrounding saturated with CO_2 vapor. The low temperature of dry ice and non-existence of liquid phase at ambient conditions facilitate a wide variety of industrial and scientific applications. For example, cryopreservation of various biopharmaceutical products like tissues [1], blood [2], and proteins [3] are traditionally carried out by cooling either directly using dry ice or by quenching in a bath of dry ice and alcohol. In the so-called spray cooling systems latent heat of phase change of dry ice is utilized in applications involving high heat flux densities such as food freezing [4] and cryogenic machining [5]. In

addition to its use as a cooling agent, dry ice has been recognized for its effective cleaning ability particularly of delicate surfaces such as mirrors of telescopes and semiconductor wafers [6]. The sublimation of dry ice, which when combined with the abrasive action of the solid particles, can dislodge and remove contaminants without leaving behind any residue. Furthermore, dry ice has exhibited potential for diverse applications beyond its common uses such as cloud seeding [7], energy harvesting [8], and closed cycle refrigeration [9].

Due to its crucial role in applications, fundamental investigation of dry ice sublimation has recently drawn a lot of attention. Interaction of sessile and self-propelling dry ice disc with a hot substrate has been experimentally and theoretically investigated to estimate crucial parameters like heat transfer rate, the sublimation rate of dry ice, and the pressure profile inside the vapor layer present between dry ice and the substrate, [10–14]. In context of thermal management, the heat transfer coefficient of the spray of dry ice particles impacting a hot solid surface

* Corresponding authors.
E-mail addresses: a.s.purandare@utwente.nl (A.S. Purandare), s.vanapalli@utwente.nl (S. Vanapalli).

Nomenclature

δ_{Th}	Thermal boundary layer [m]	$\overrightarrow{j}_v$	Vapor diffusion mass flux [kg/(m^2 s)]
$\dot{m}''_{sub}$	Mass flux of the sublimated vapor [kg/(m^2 s)]	$\overrightarrow{v}$	Mass averaged velocity vector of gas mixture [m/s]
ν_{CO_2}	Volume fraction of CO_2 vapor in gas mixture	D	Diffusion coefficient of CO_2 in N_2 [m^2/s]
$\mathscr{L}$	Specific latent heat of dry ice [J/kg]	g	Acceleration due to gravity [m/s^2]
$\mathscr{M}_v$	Mass fraction of CO_2 vapor in gas mixture	h	Heat transfer coefficient [W/(m^2 K)]
CO_2	Carbon dioxide	k_g	Thermal conductivity of gas mixture [W/(m K)]
N_2	Nitrogen	k_s	Thermal conductivity of dry ice sphere [W/(m K)]
Ω	Diffusion integral	m_s	Mass of dry ice sphere [kg]
ρ'	Density of CO_2 gas in the mixture [kg/m^3]	M_{CO_2}	Molecular weight of CO_2 [g/mol]
ρ_g	Gas density [kg/m^3]	M_{N_2}	Molecular weight of N_2 [g/mol]
ρ_v	Density of CO_2 vapor [kg/m^3]	p	Pressure of gas mixture [atm]/[bar]
ρCO_2	Total density of CO_2 gas [kg/m^3]	R	Universal gas constant [J/(mol K)]
σ	Stefan-Boltzmann constant [W/(m^2 K^4)]	r_s	Radius of dry ice sphere [m]
$\sigma_{CO_2-N_2}$	Collision diameter [Å]	T_g	Temperature of gas mixture [K]
$\mathbf{n}$	Normal vector at the dry ice sphere surface	T_s	Temperature of dry ice sphere [K]/[°C]
$\overrightarrow{j}_g$	Gas diffusion mass flux [kg/(m^2 s)]	$T_{g,\infty}$	Far-field temperature of gas mixture [K]
		Bi	Biot number
		IR	Infrared

has been experimentally evaluated by temperature measurements [15] and theoretically predicted by numerically modeling the two phase solid-vapor flow from a nozzle inlet to a heat source surface [16,17].

The aforementioned studies have been conducted on the premise that the sublimation temperature of dry ice under atmospheric pressure is −78.5 °C. However, it must be noted that this assumption is conditionally precise as this temperature is only valid in a stationary state, where the dry ice is exposed to an environment that is saturated with its own vapor. In practical scenarios, however, dry ice is predominantly utilized in an unsaturated atmosphere, and therefore, it is expected to undergo sublimative cooling similar to a liquid droplet that experiences evaporative cooling in an unsaturated atmosphere. As a result, dry ice will reach a thermodynamic wet bulb temperature that is dependent on the concentration and pressure of the gas present in the surroundings. Failing to account for sublimative cooling can lead to significant discrepancies in predicting the rate of sublimation of dry ice, particularly when a substantial reduction in temperature occurs at the dry ice's surface.

Significant research has been conducted to experimentally and theoretically examine the influence of vapor concentration and pressure on the evaporative cooling of liquid droplets by exploring the interplay of heat and mass transfer phenomena at the interface between the droplets and the surrounding gaseous medium [18,19]. However, this has not been extensively studied for sublimating dry ice, with only two studies conducted around three decades ago to study the influence of the ambient conditions on the sublimation of dry ice pellets for cloud seeding application [7,20]. In particular, the effect of ambient temperature, air quality, and relative air velocity on the number of water ice crystals around dry ice pellets, and the sublimation rate of pellets has been measured. However, the effect of ambient on the surface temperature of dry ice pellets has only been briefly described in the appendices of their respective works. Fukuta et al. [20] empirically calculated the surface temperature of dry ice which varied from −99.7 °C to −102.6 °C for a dry ice pellet of 0.9 cm diameter placed in an environment of 0.82 atm pressure and 9.14 msec^{-1} air velocity, and ambient temperature varying in the range of 25 °C to −12 °C. Kochtubajda and Lozowski [7] measured the temperature of cylindrical dry ice pellets exposed to an air stream in a wind tunnel as −95.7 ± 0.3 °C. However, the ambient concentration in these experiments has not been well controlled and therefore, its influence on the dry ice temperature is also not reported. Finally, to the author's knowledge, there is no further literature providing data for dry ice sublimation and the associated saturation temperature for varying ambient conditions in terms of far-field pressure and concentration.

In the present work, the influence of the far-field ambient pressure and CO_2 concentration on the sublimation temperature of a dry ice sphere is experimentally and theoretically examined. The final outcome is presented in the form of an extended phase diagram for CO_2, which displays the solid-vapor coexistence lines for various far-field CO_2 concentrations as well as the coexistence curve from the standard phase diagram. Additional experiments are conducted using spheres of different sizes to assess the impact of sphere size on the sublimation temperature of dry ice. Furthermore, a simplified one-dimensional analytical model that considers heat and mass transport in the surroundings of a dry ice sphere is developed to predict the sublimation temperature based on the far-field pressure and CO_2 concentration. Theoretical predictions are found to be in good agreement with experimental results. The present study provides extensive experimental and theoretical data for sublimation temperature under varying ambient conditions, which can lead to a significant improvement in modeling approaches involving dry ice by accurately reflecting its actual temperature in relevant problems.

2. Experimental

The investigation carried out in this paper is supported by thorough comparison with experiments. In order to accurately measure the sublimation temperature of dry ice subjected to various ambient conditions, a setup is designed and built with adequate control on ambient pressure and CO_2 concentration. The schematic of the experimental setup is shown in Fig. 2. It basically consists of two parts, namely, a testing unit housing a dry ice sphere surrounded by a controlled ambient, and a control unit which maintains desired pressure and CO_2 concentration in the test section during the time period of an experiment.

2.1. Test section

The test section on the right side of Fig. 1 consists of a cross-shaped KF vacuum flange housing a dry ice sphere. The flange has four ports, two each in the vertical and horizontal direction. The ports along the horizontal direction are equipped with viewing windows to observe the dry ice sphere during sublimation. The dry ice sphere is suspended at the tip of a thin wire E-type thermocouple (0.25 mm diameter). An additional E-type thermocouple is placed inside the flange near its top port to measure the temperature of the incoming gas. Both the thermocouple wires are mechanically fixed and sealed in a KF flange pass-through to
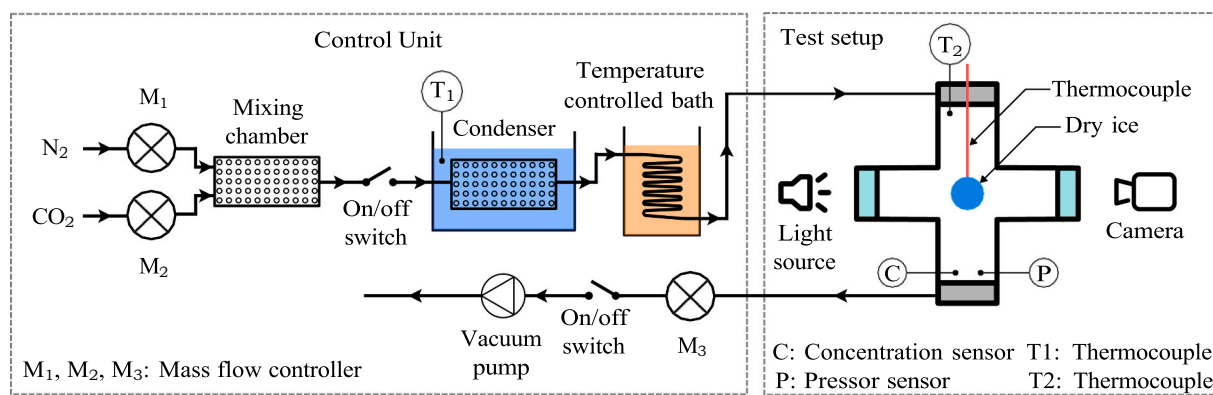
Fig. 1. Schematic of the experimental setup to measure the sublimation temperature of a dry ice sphere suspended in ambient of controlled pressure and CO_2 concentration.

keep the test section airtight. Thermocouples are calibrated using three known temperature points: ice-water slush at 0 °C, solid-liquid nitrogen slush at −210 °C, and dry ice in pure CO_2 environment at −78.5 °C. The CO_2 concentration in the test section is measured using a non-dispersive IR-absorption sensor [21], calibrated to an accuracy ∼ 1%, placed at the bottom port of the flange. It should be noted that the output of the CO_2 sensor is influenced by the pressure inside the test section, which is compensated for using a polynomial provided by the manufacturer [21] in order to minimize its impact on measurement accuracy. The operational pressure limit within the test section is thus determined by the accuracy of the pressure compensation, in addition to the mechanical constraints of the CO_2 sensor. As a result, the operating pressure during the experiments conducted in the test section ranges from 600 mbar to 1.3 bar. Further details regarding the control unit of the experimental setup, responsible for regulating the concentration and pressure within the test section, is elaborated in the subsequent subsection.

2.2. Control unit

The control unit shown on the left of Fig. 1 conditions the flow of gas entering and refreshing the test section at a volume flow rate of 1 L/min, moderate enough to not significantly impact the measured temperature data. A supply of pure nitrogen (N_2 5.0) and carbon dioxide (CO_2 2.7) gas is controlled by a pair of Bronkhorst mass flow controllers (M1, M2), which regulate the flow of these gases depending on the desired CO_2 concentration inside the test section. The two gases from M1 and M2 first pass through a mixing chamber to ensure a homogeneous mixture of these two gases. The impurity, mainly water vapor, present in the gases (5 mg/L and 150 mg/L for N_2 and CO_2, respectively) is removed in the condenser maintained at ∼ -60 °C. Before the gas mixture enters the test section, it passes through a heat exchanger in a temperature-controlled bath to ensure the gas mixture temperature is ∼ 20 °C.

The pressure inside the test section is controlled using a vacuum pump attached to the bottom port of the cross-shaped flange in combination with an appropriate setting of the mass flow controller, M3, present at the exit of the test section. M3 is PID controlled that maintains the pressure inside the chamber at a desired value (±1 mbar) by the balance of the volume flow into and out of the test section. The active control of the pressure inside the test section is essential, without which the pressure will drift from its set value due to the changes in outflow concentration and sublimation of dry ice. The pressure inside the test section is measured using the MKS Baratron type 626 A pressure sensor [22].

2.3. Dry ice sphere

Dry ice in the form of snow is obtained from expanding high-pressure liquid CO_2 (∼ 57 bar at 20 °C) through an orifice to the atmospheric pressure. The flakes of the dry ice snow are compressed via a piston in a spherical mold of the required diameter, while the thermocouple wire is partially inside the mold centre during compression. The spherical mold-piston arrangement and the solid dry ice sphere having a 10 mm initial radius produced during experiments are shown in Fig. 2 a) and b), respectively.

The dry ice spheres obtained using this technique had an effective density in the range of 835 kg/m^3 to 955 kg/m^3, evaluated from the measured initial mass of the sphere and its known initial volume. This broad spectrum of the sphere's effective density is due to the manual compression of snow via the piston, the force on which varies during different runs of the experiment. Therefore, the dry ice sphere's average porosity evaluated from the effective to the actual density ratio is ∼ 35%.

2.4. Experimental procedure

During the startup of the experimental setup, the vacuum pump is switched on to first depressurize the test section to ∼ 7–10 mbar to minimize the residual uncontrolled composition of the gas initially present in the test section. Next, the desired CO_2 concentration and the pressure are set in a LabVIEW program which controls the opening or closing of the mass flow controllers M1, M2, and M3 to maintain concentration and pressure conditions inside the test section during the period of an experiment. With these conditions, the test section is flushed with the gas of set CO_2 concentration and pressure for ∼ 10 min so that the total volume of the experimental setup (∼ 2 L) is refreshed several times and ensure homogeneous initial conditions monitored by
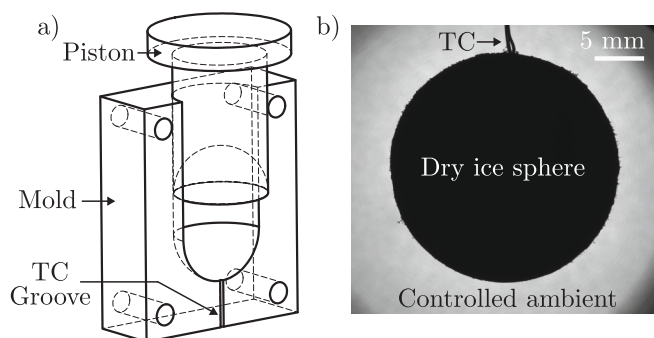

Fig. 2. a) Schematic of the mold cut section and piston assembly used to produce a dry ice sphere. The groove in the mold is to insert thermocouple wire into the mold before dry ice snow is compressed. b) A picture of a dry ice sphere (radius = 10 mm), suspended on the thermocouple wire (TC) inside the test section, taken at the start of an experiment.

the concentration and pressure sensor present inside the test section. The dry ice sphere is then produced, its mass is measured, and then immediately suspended in the test section.

Each experiment starts with 100%vol CO_2 concentration in the test section to check the dry ice sublimation temperature is equal to its saturation temperature at a given pressure (e.g. -78.5 °C at 1 atm pressure). As time progresses, the CO_2 concentration is lowered, and the corresponding sublimation temperature is measured. This procedure of reducing concentration is carried out in the steps of 20% vol until 0%vol CO_2 concentration inside the test section. So in an experiment, we obtain 6 data points of the dry ice sublimation temperature corresponding to the 6 different values of CO_2 concentration at a given pressure in the test section. This experimental procedure is repeated for other pressures varying from 600 mbar to 1.3 bar in the steps of ~ 100 mbar. The E-type thermocouple is securely positioned inside the dry ice sphere to measure the sublimation temperature. The duration for which the thermocouple maintains contact with the dry ice sphere depends on the quality of its placement at the center of the sphere, and the ambient conditions. In the optimal case, the thermocouple remains in contact with the dry ice for approximately 40 min before the sphere loses contact with the tip of the thermocouple due to sublimation. The experiment is repeated 3 times for a given pressure to check repeatability. Additionally, a few sets of experiments are performed with the starting CO_2 concentration equal to 0%vol and increasing it back to 100%vol in the steps of 20%vol to ensure the absence of hysteresis in the measurements.

2.5. Errors and uncertainty in measurements

In the process of measuring the sublimation temperature using the thermocouple wire supporting the dry ice sphere at its tip, an error of 0.3 °C is estimated. This estimation is based on the variability in temperature observed during the calibration procedure. Additionally, temperature drift of ~ 0.3 °C is during the dry ice lifetime. This is postulated to result from the degradation of contact between the thermocouple tip and the dry ice. This degradation stems from a minor parasitic heat load transmitted through the thermocouple wire to the dry ice. Notably, this error is most pronounced in data points collected towards the conclusion of an experiment. Nonetheless, due to the challenge of precisely controlling the extent of junction contact with the dry ice, this error is treated as a consistent factor across all measurement points.

The inaccuracy in the test section's pressure, as measured by the pressure sensor, is on the order of $\mathcal{O}(1 \text{ mbar})$. According to the standard phase diagram of CO_2, a variation in pressure by $\mathcal{O}(1 \text{ mbar})$ corresponds to an alteration in the sublimation temperature of dry ice by $\mathcal{O}(0.01 \text{ K})$ at a 100%vol concentration of CO_2. Consequently, the temperature measurement error stemming from the imprecise pressure measurement is a magnitude lower compared to the previously determined thermocouple error, thus rendering it negligible.

The accuracy of the CO_2 concentration sensor, employing non dispersive IR absorption, relies on quantifying the number of molecules within a fixed volume. However, its accuracy is susceptible to the far-field pressure and temperature conditions of the given volume, unless suitable compensations are implemented to counter these effects. In the context of this investigation, the far-field temperature is held constant to approximately 20 °C, while variations in pressure are introduced within the test section. The extent of the influence of pressure changes on the sensor's accuracy depends on the specific concentration of the gas mixture. To address these considerations, a compensation polynomial supplied by the manufacturer is employed to convert the sensor's output. This compensation methodology proves adequately effective within the pressure range of 600 mbar to 1.3 bar. Within this pressure span, the errors incurred at both extremely low and high CO_2 concentrations remain below 4%, while for nominal CO_2 concentrations, the error is contained within 1%. Comprehensive details regarding the compensation polynomial are available in the datasheet furnished by the sensor's supplier [21].

3. Theory

In this section, we focus on the theoretical estimation of the sublimation temperature of a dry ice sphere in equilibrium with N_2-CO_2 gaseous mixture of a given pressure and CO_2 concentration surrounding the dry ice. This situation is schematically shown in Fig. 3 and mathematically described using a quasi-steady sublimation of a solid sphere of mass m_s, temperature T_s, and specific latent heat $\mathscr{L}$ suspended in a binary gaseous mixture of CO_2 and N_2 having thermal conductivity k_g and diffusion coefficient D. The binary gas system is assumed ideal, whose thermal conductivity and diffusion coefficient depend on the ambient temperature and pressure. While the temperature dependence of the thermal conductivity of the gaseous mixture for a given pressure is obtained using the commercial software REFPROP [23], the following expression for the diffusion coefficient is used based on Chapman and Enskog's theory [18,24]:

$$D = 1.86 \cdot 10^{-7} \frac{T_g^{\frac{3}{2}}(1/M_{CO_2} + 1/M_{N_2})^{\frac{1}{2}}}{p \, \sigma_{CO_2-N_2}^2 \, \Omega} \quad (\text{m}^2/\text{s}), \tag{1}$$

where M_{CO_2} and M_{N_2} are the molecular weights of CO_2 and N_2 gas, T_g is the absolute temperature of the mixture in Kelvin, p is the pressure in atmospheres, $\sigma_{CO_2-N_2}$ is the collision diameter expressed in angstroms, and Ω is a dimensionless quantity known as the diffusion integral whose value is of the order 1 and is weakly dependent on the temperature of the mixture [24,25]. In this case, its value is assumed to be 1.05, evaluated at the mean temperature of the far-field and dry ice.

The far-field pressure and temperature of the gaseous mixture surrounding the dry ice sphere are assumed constant as the ambient is actively replenished and controlled at the required far-field conditions during an experiment. The transport of the sublimated CO_2 vapor from the surface of the dry ice sphere to far-field, under the steady state, is governed by the equation

$$\nabla \cdot (\rho_v \, \vec{v}) + \nabla \cdot \vec{j}_v = 0 \tag{2}$$

[25], where ρ_v, $\vec{v}$, and $\vec{j}_v$ are the vapor concentration, mass averaged velocity vector of the mixture, and the vapor diffusion mass flux, respectively. The mass flux of the sublimated vapor $\left(\dot{m}''_{sub} \right)$ due to convective and diffusive transport is written as
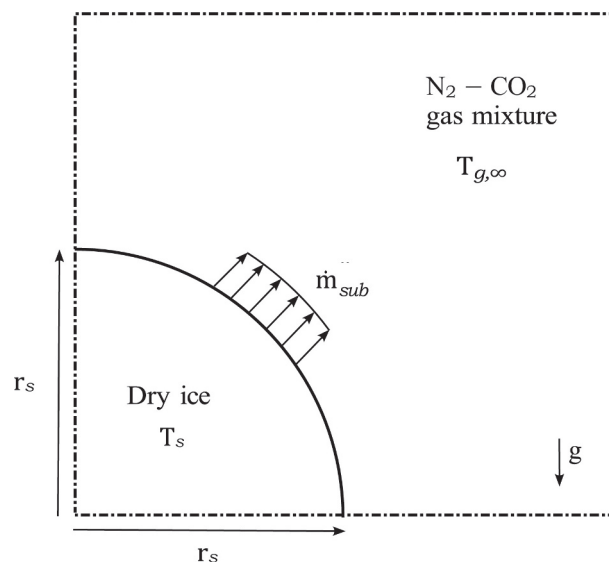

Fig. 3. Schematic of the quarter of a dry ice sphere sublimating in a mixture of N_2-CO_2 gas at a fixed far-field pressure and temperature.

$$\dot{m}''_{sub} = \rho_v \vec{v} + \vec{j}_v. \tag{3}$$

In addition to the diffusion of CO_2 vapor away from the dry ice surface, the N_2 molecules also diffuse towards the dry ice's surface due to the concentration gradient. However, since N_2 is not soluble in the dry ice, the concentration of N_2 at the dry ice surface must eventually disappear. As a result, a bulk gas flow, known as the Stefan flow, is generated near the interface, carrying N_2 molecules away from the dry ice surface at the same rate as N_2 diffusion. The Stefan velocity can be estimated from the expression for the mass flux of N_2 (Eq. (4)), which is equal to zero under the assumption that the dry ice surface is impervious to N_2 gas.

$$\rho_g \vec{v} + \vec{j}_g = 0 \tag{4}$$

Since the sum of mass fluxes for species diffusing in a stationary medium is zero ($\sum_i \vec{j}_i = 0$), the Stefan velocity can be expressed in terms of diffusion mass flux of CO_2 vapor as

$$\vec{v} = -\frac{\vec{j}_g}{\rho_g} = \frac{\vec{j}_v}{\rho_g}, \tag{5}$$

which in turn is used to rewrite Eq. (3) as

$$\dot{m}''_{sub} = \vec{j}_v \left(\frac{\rho_v}{\rho_g} + 1 \right). \tag{6}$$

The diffusional vapor mass flux, $\vec{j}_v$, is eliminated using Fick's law, and Eq. (6) is rewritten in one dimensional form as

$$\dot{m}''_{sub} = -D \frac{d\rho_v}{dr} \left(\frac{1}{1 - \mathcal{M}_v} \right), \tag{7}$$

where $\mathcal{M}_v = \rho_v / \rho$ represents the mass fraction of CO_2 vapor.

Energy transfer between the ambient and the dry ice sphere during its sublimation occur through sublimative heat transfer, heat conduction, and radiation in the gas phase. The resulting energy balance at the interface between dry ice and the ambient is described by the following equation

$$n \cdot (-k_s \nabla T_s) = \dot{m}''_{sub} \mathcal{L} - n \cdot (-k_g \nabla T_g) + \sigma \varepsilon \left(T_s^4 - T_g^4 \right), \tag{8}$$

where k_s, n, and ε are the thermal conductivity of dry ice, surface normal vector at the sphere surface, and emissivity of the dry ice surface. The first term in (8) is neglected by assuming that temperature gradients inside the dry ice sphere have been decayed in the time taken by the dry ice sphere to reach equilibrium with the ambient. This assumption is valid for small Biot number ($Bi = h r_s / k_s$), which in this case is calculated to be 0.5 for a dry ice sphere radius (r_s) of 10 mm, thermal conductivity (k_s) of 0.2 W/(m K), and the heat transfer coefficient between dry ice and ambient (h) of the order of 10 W/(m^2 K). Furthermore, the heat transfer due to radiation between ambient and dry ice surface is neglected as its magnitude is an order of magnitude lower than the magnitude of the heat conducted via the ambient to the dry ice surface, $\sigma \left(T_s^4 - T_g^4 \right) / \overline{k}_g \frac{T_s - T_g}{\delta_{Th}} \sim 0.3$, where $\sigma = 5.67 \times 10^{-8}$ W/(m^2 K^4) is the Stefan-Boltzmann constant, $\overline{k}_g \sim 12.5$ mW/(m K) is the thermal conductivity of the gas mixture evaluated at the mean of gas temperature ($T_g \sim 293$K) and dry ice temperature ($T_s \sim 195$K). For a conservative estimate of this assumption, the emissivity of the dry ice surface is assumed to be 1, and the thickness of the thermal boundary layer (δ_{Th}) to be of the order of 1 mm. After considering the aforementioned assumptions, the Eq. (8) is simplified and rewritten in one-dimensional form as

$$\dot{m}''_{sub} \mathcal{L} = k_g \frac{dT_g}{dr}. \tag{9}$$

Contrary to the common practice, transport properties, namely, the thermal conductivity and mass diffusivity in the gas domain are considered temperature dependent in this work for evaluating the density of vapor as a function of temperature from the following equation

$$\frac{d\rho_v}{dT_g} = -\frac{k_g(T_g)}{\mathcal{L} D(T_g)} (1 - \mathcal{M}_v), \tag{10}$$

which is obtained from Eqs. (7) and (9). Both the thermal conductivity and the diffusion coefficient of the gas phase are increasing functions of temperature, namely,

$$k_g = A T_g + B \tag{11}$$

and

$$D = C T_g^{3/2}. \tag{12}$$

While the constants A and B are evaluated by fitting a straight line to the data of thermal conductivity obtained from the commercial software REFPROP [23], the value of C is evaluated by grouping the constant terms of Eq. (1) for a given gas composition and far-field pressure.

Using the aforementioned temperature-dependent expression for the transport properties, Eq. (10) is integrated, leading to the subsequent expression

$$\rho_v = -\frac{2(A T_g - B)}{\mathcal{L} C \sqrt{T_g}} (1 - \mathcal{M}_v) + \text{constant}. \tag{13}$$

The integration constant is determined using the known far-field vapor density ($\rho_{v,\infty}$) and temperature ($T_{g,\infty}$). Subsequently, the vapor density diffused from the surface of dry ice towards the far-field, in relation to the temperature of the gas mixture, can be expressed as follows

$$\rho_v = \rho_{v,\infty} + \frac{2(1 - \mathcal{M}_v)}{\mathcal{L} C} \left(\frac{A T_{g,\infty} - B}{\sqrt{T_{g,\infty}}} - \frac{A T_g - B}{\sqrt{T_g}} \right). \tag{14}$$

In addition to the vapor diffused from the dry ice surface, the density of the CO_2 gas originally present in the mixture is calculated using the ideal gas law ($\rho' = p M_{CO2} / R T_g$), where p is total pressure and $R = 8.314$ J/(mol K) is the universal gas constant. The total density of CO_2 gas surrounding the dry ice sphere is then evaluated as

$$\rho_{CO_2} = (1 - \nu_{CO_2}) \rho_v(T_g) + \nu_{CO_2} \rho'(T_g), \tag{15}$$

where ν_{CO_2} is the volume fraction of CO_2 in the mixture. The factor $1 - \nu_{CO_2}$ appears in the first term of Eq. (15) because the CO_2 vapor from the dry ice surface diffuses only in the fraction of N_2 gas present in the mixture. The second term in the Eq. (15) represent the density of the CO_2 present in the fraction of the volume originally occupied by it in the mixture.

Finally, the Eq. (15), for a given pressure and varying CO_2 concentration levels of the mixture, is plotted on the phase diagram, showing the variation of vapor density instead of vapor pressure as a function of temperature, of CO_2. The curve representing the result of Eq. (15) must satisfy the far-field density as well as the vapor density at the surface of the dry ice, and therefore the temperature at which the curves intersect is taken to be the sublimation temperature of dry ice surrounded in a mixture of N_2-CO_2 gas at the corresponding CO_2 concentration. An example of this graphical evaluation of the sublimation temperature of dry ice is shown in Fig. 4. The solid line represents the saturation vapor density of CO_2, ρ_{sat}, as a function of temperature. This is obtained by expressing Clausius-Clapeyron relation of vapor pressure ([26]) in the form of vapor density using the ideal gas law. The dashed lines are the density of the CO_2 calculated using Eq. (15) as a function of temperature evaluated for different far-field concentration and a fixed far-field
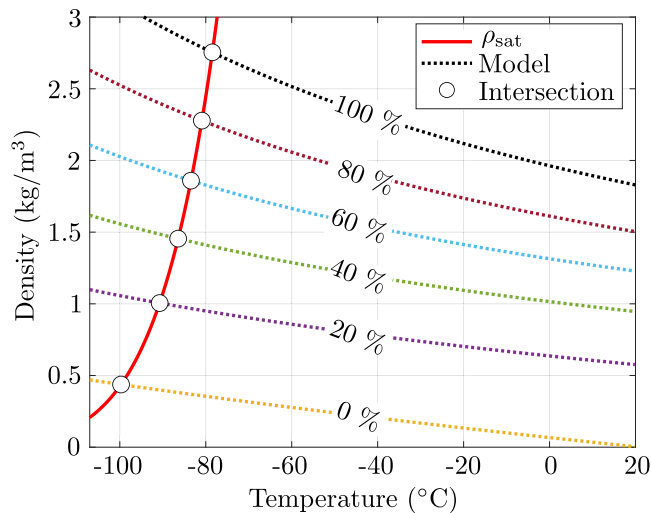
Fig. 4. CO_2 vapor density (y-axis) as a function of temperature (x-axis). The dashed lines represent the total density of CO_2 calculated from Eq. (15) for different CO_2 concentration at 1 bar total pressure. The intersection points, shown using circular markers, represent the predicted sublimation temperature of dry ice at the corresponding concentration level.

pressure and temperature of 1 bar and 20 °C, respectively.

At 100% CO_2 concentration, $\nu_{CO_2} = 1$ and as a result the first term on the right hand side of the Eq. (15) is zero implying no contribution of the diffusive transport of vapor from dry ice surface. The result of Eq. (15) plotted for this situation i.e., the dashed line corresponding to 100% CO_2 concentration in Fig. 4 intersects the saturation density curve at a temperature of -78.5 °C. This is the value of the sublimation temperature commonly quoted in literature which is true only if the dry ice is sublimating in the surrounding saturated with CO_2 vapor. For concentrations lower than 100% in the surroundings of dry ice ($\nu_{CO_2} < 1$), the contribution of the diffusive term in Eq. (15) becomes relevant due to which the result of Eq. (15), for the same far field temperature, intersects the saturated vapor density curve at lower temperature as seen in Fig. 4. At 0% CO_2 concentration ($\nu_{CO_2} = 0$), i.e., when dry ice is surrounded by only N_2 gas, the diffusive term of Eq. (15) alone contributes to the total density of CO_2. For this case, the dashed line corresponding to 0% CO_2 concentration in Fig. 4 satisfies the far field condition of zero CO_2 density at 20 °C and intersects the saturated vapor density curve at a temperature of -99.7 °C which is the predicted value of the sublimation temperature of dry ice surrounded by a gas having zero CO_2 concentration.

In general, the sublimation temperature of dry ice is coupled to the concentration of CO_2 in the surrounding medium which is important to consider while investigating thermal processes involving dry ice which otherwise will result in significant deviation up to 20 °C from the commonly quoted value of dry ice's sublimation temperature. In the subsequent sections, the theoretical results are validated by comparing the predicted values of the sublimation temperature, obtained from the intersection points shown in Fig. 4, with the measured values for different CO_2 concentration, pressure and initial size of the dry ice sphere.

4. Results

Using the setup described in Section 2, the influence of CO_2 concentration and ambient pressure on the sublimation temperature of dry ice is studied. At first, the measured sublimation temperature for a fixed normal atmospheric pressure and varying levels of far-field CO_2 concentration is discussed. In the subsequent subsections, the measured and predicted values of the sublimation temperature for varying CO_2

concentration levels, ambient pressure, and sphere dimension are presented. Furthermore, the solid-vapor coexistence lines for different far-field CO_2 concentrations are evaluated and compared with the coexistence line present on a standard phase diagram of CO_2. Lastly, it is shown for lower concentration levels, an accurate estimate of the sublimation temperature of dry ice cannot be made by simply considering partial pressure corresponding to a given far-field CO_2 concentration.

4.1. Influence of the far-field CO_2 concentration

Fig. 5 a) displays the experimental results obtained for the sublimation temperature of a dry ice sphere of radius $r_S = 10$ mm suspended in an ambient environment maintained at a pressure of normal atmospheric pressure (~ 1.013 bar). The concentration of CO_2 in the far-field is systematically varied from 100%vol to 0%vol in increments of 20% vol. It is observed that the sublimation temperature of dry ice is measured as -78.5 °C when the ambient surrounding the dry ice sphere is saturated with CO_2 gas (100%vol) at normal atmospheric pressure, which is in agreement with the expected value. The concentration of CO_2 in the inflow gas entering the test section is subsequently reduced to 80%vol after approximately 210 s. The CO_2 concentration measured at the exit of the test section takes approximately 290 s to stabilize near the inflow concentration. During this process, the dry ice sphere immediately responds to the change in CO_2 concentration in its surroundings. Its temperature reduces due to sublimative cooling until it reaches a thermodynamic steady-state wet-bulb temperature of $\sim$ -80.5 °C. This process of lowering the CO_2 concentration inside the test section continues until its lowest value of 0%vol CO_2 concentration of the inflow gas, and the sublimation temperature at this concentration level is measured to be $\sim$ -97.3 °C. This temperature is $\sim$ 19 °C lower than the sublimation temperature of dry ice typically reported in the literature at saturated conditions. It can be observed from Fig. 5 that the measured value of the CO_2 concentration is higher than the concentration of the inflow gas by $\sim$ 3–4%vol. This concentration discrepancy could be ascribed to the CO_2 concentration of the sublimated vapor measured by the sensor, located at the exit of the test section, in addition to the CO_2 concentration of the inflow gas. To simplify and facilitate analysis, the results presented in the subsequent sections correspond solely to the CO_2 concentration of the inflow gas.

In Fig. 5 b), the measured values of the sublimation temperature are shown for increasing levels of the far-field CO_2 concentration from 0% vol back to 100%vol at normal atmospheric pressure. It can be seen by comparing Fig. 5 a) and b) that the dry ice sublimation temperatures are similar for similar concentration levels for both cases, confirming the robustness of the experiments. The exact values of the dry ice sublimation temperature, i.e. the steady-state temperature values in Fig. 5 a) and b), at different concentration levels for both cases are listed in Table 1. The differences in the measured values for a given concentration in both cases can be attributed to the thermocouple error and contact degradation between the thermocouple tip and the dry ice sphere.

4.2. Impact of dry ice sphere size

The results presented in the previous section are for the dry ice sphere with an initial radius of 10 mm. To investigate the effect of the sphere size on its sublimation temperature, a sphere with an initial radius of 5 mm was also studied for three different far-field CO_2 concentrations, specifically 100%vol, 60%vol, and 20%vol. Fig. 6 shows the measured steady-state sublimation temperature for the two different sphere sizes at ~ 1.013 bar pressure for the different CO_2 concentrations. As observed in the previous section, the sublimation temperature of dry ice decreases with decreasing far-field CO_2 concentration, resulting in a larger difference between the sublimation temperature at a given concentration and at the saturated condition. The sublimation temperature change is found to be similar for both the 5 mm and 10 mm spheres, indicating that the effect of the sphere size is negligible when
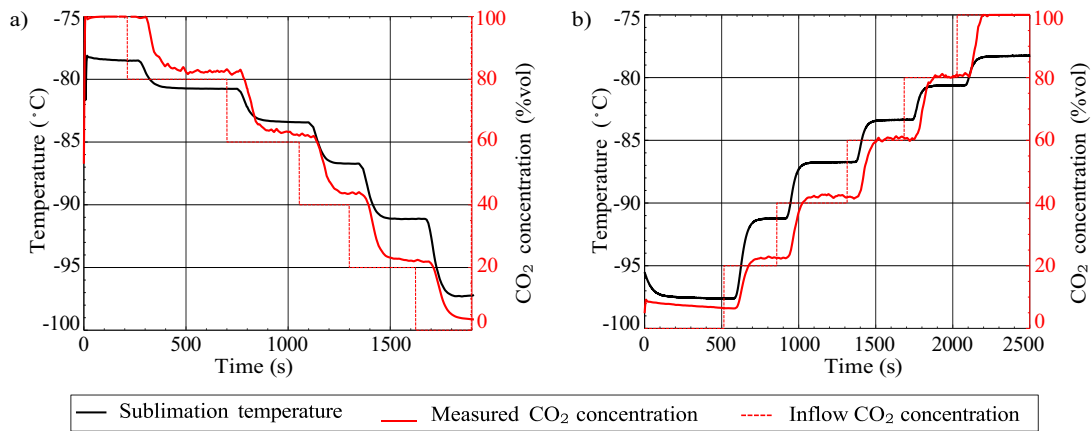
Fig. 5. Measured values of the sublimation temperature (left y-axis) of a dry ice sphere (r_s = 10 mm) suspended in the test section maintained at ~ 1.013 bar pressure and CO_2 concentration (right y-axis) varying **a)** from 100%vol to 0%vol in the steps of 20%vol and **b)** from 0%vol back to 100%vol in the steps of 20%vol.

Table 1

Comparison of the dry ice sublimation temperature (in °C) measurements under varying far-field concentrations of CO_2, ranging from 100%vol to 0%vol, with the measurements obtained when the concentration levels were varied in the reverse order, i.e., from 0%vol to 100%vol.

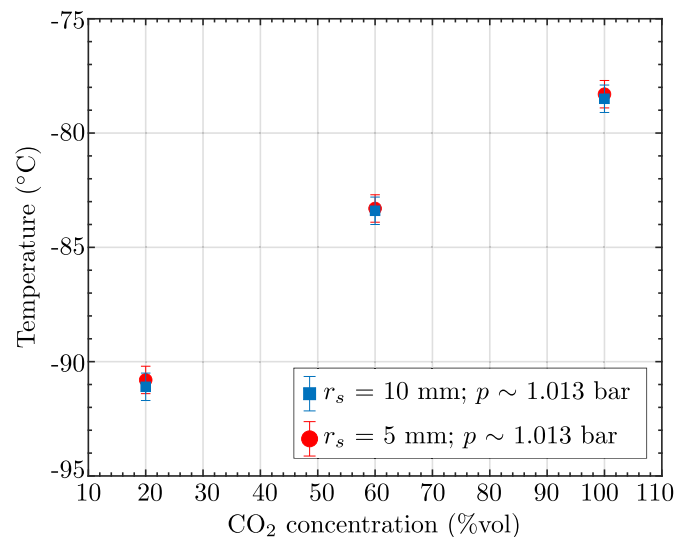| Start point ⇒	100%vol	0%vol
Set-point ⇓		
%vol	-78.5	−78.3
80%vol	−80.7	−80.6
60%vol	−83.4	−83.4
40%vol	−86.7	−86.7
20%vol	−91.1	−91.2
0%vol	−97.3	−97.6

Fig. 6. The measured sublimation temperature (y-axis) as a function of far-field CO_2 concentration (x-axis) for two different sizes of dry ice spheres.

the dry ice is in thermal equilibrium with its surroundings. Hence, the experimental and theoretical results presented in the subsequent sections consider only the dry ice sphere with an initial radius of 10 mm.

4.3. Influence of ambient pressure

The influence of the ambient pressure on the measured and predicted values of the dry ice sublimation temperature for various far-field CO_2

concentration is shown in Fig. 7. The results presented in this figure are discussed in two parts; i) the influence of CO_2 concentration on the steady-state sublimation temperature of dry ice at a given ambient pressure, and the ii) the influence of the ambient pressure on the steady-state sublimation temperature of dry ice at a given CO_2 concentration.

i) The variation of the dry ice sublimation temperature with the far-field CO_2 concentration is similar for all ambient pressures, i.e., it decreases with a reduction in concentration from its highest value, at 100%vol concentration, to its lowest value, at 0%vol concentration. It can be seen from Fig. 7 that the predicted values of the sublimation temperature are in good agreement with the measured values, except for the 0%vol concentration where the measured value is approximately 2–3 °C higher than the predicted value. This discrepancy is presumably due to the accumulation of a small amount of CO_2 vapor inside the test section during dry ice sublimation, leading to a higher actual CO_2 concentration than the inflow concentration used in the model. For example, when the inflow concentration of CO_2 is set to 0 during an experiment, it is expected that pure N_2 gas reaches the
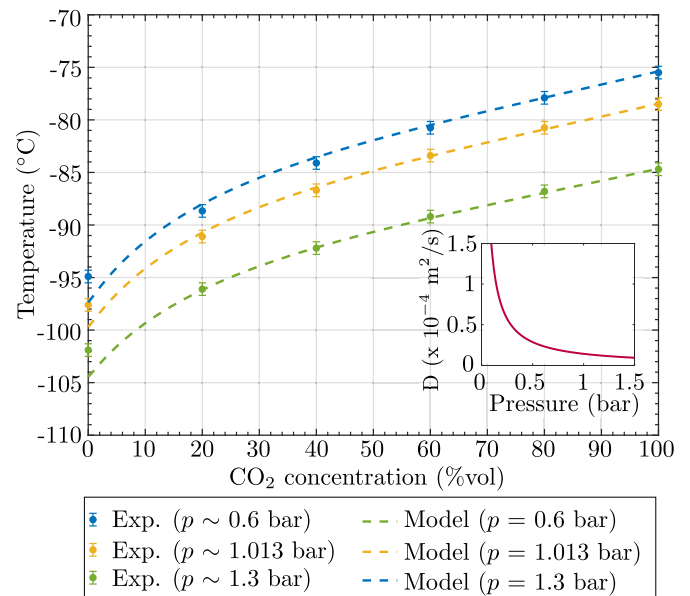

Fig. 7. Influence of the far-field CO_2 concentration (x-axis) and pressure on measured and predicted dry ice sublimation temperature (y-axis). The inset of the figure shows the variation of the diffusion coefficient (D) of CO_2 vapor in N_2 gas as a function of pressure.

test section and surrounds the dry ice sphere. But the actual concentration of CO_2 (2–3%vol) can be higher in the test section due to accumulation of the sublimated vapor from the dry ice surface even though the test section is continuously refreshed with the inflow gas. Since the inflow concentration (0%vol) is used in the model, the predicted concentration gradient between the dry ice sphere and the ambient is higher than in the experiments, leading to over-prediction of sublimative cooling and under-prediction of sublimation temperature for the 0%vol concentration.

ii) The influence of atmospheric pressure on the dry ice sublimation temperature for a given far-field concentration can also be seen in Fig. 7. The results indicate that, for all values of the far-field CO_2 concentration, both the measured and predicted sublimation temperature reduces as the pressure decreases. This trend can be explained by the pressure-dependent diffusion coefficient of CO_2 in N_2 gas, which is represented graphically in the snippet of Fig. 7 and described by Eq. (1). Specifically, as the ambient pressure decreases, the diffusion coefficient of CO_2 increases, resulting in increased sublimation from the dry ice surface. This, in turn, enhances sublimative cooling of the dry ice sphere and leads to a lower sublimation temperature of dry ice.

4.4. Extended phase diagram

The comprehensive overview of both experimental and theoretical results of the dry ice sublimation temperature at various far-field CO_2 concentrations and pressures is shown in Fig. 8. The three sets of data, namely, the measurements, predictions, and the solid-vapor coexistence curve from the standard phase diagram based on Clausius-Clapeyron theory [26] coincide at 100%vol CO_2 concentration. This agreement with the Clausius-Clapeyron theory, which represents the saturated condition of CO_2, serves as a benchmark for comparison and confirms the validity of the models and experimental results.

The value commonly cited for dry ice sublimation temperature in the literature is -78.5 °C or 194.65 K under standard atmospheric conditions. However, this value is accurate solely for dry ice within an environment saturated with 100% CO_2 concentration at 1.013 bar pressure. In real-world applications involving dry ice, the surrounding atmosphere is generally not saturated with its vapor. Hence, for engineering purposes, it's essential to include data pertaining to the sublimation
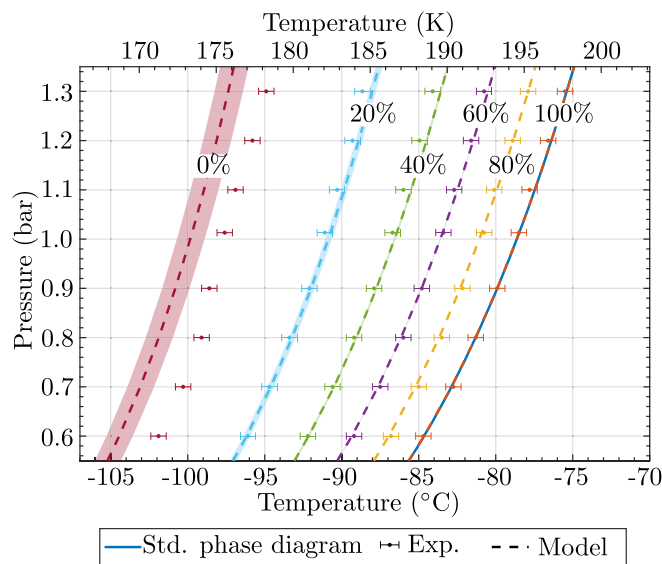
temperature of dry ice in relation to ambient pressure for different levels of far-field CO_2 concentration across the phase diagram. This information is depicted in Fig. 8, showcasing the sublimation temperature data for varying CO_2 concentrations from 80% vol to 0% vol, in increments of 20% vol. It's noticeable that for all concentration levels, the changes in measured sublimation temperature for different ambient pressures resemble the variations seen in the standard phase diagram at 100% CO_2 concentration. Consequently, these points on the graph correspond to the coexistence curves for their respective CO_2 concentration levels.

The sublimation temperature values of dry ice predicted for different ambient pressures and concentrations exhibit good agreement with the experimental data, except in the case of 0% vol CO_2 concentration as seen in Fig. 8. The deviation in this instance can be attributed to the accumulation of a small amount of CO_2 vapor within the test section, causing a minor increase in the far-field CO_2 concentration (around 2–3% vol) compared to the set value (0% vol). This concentration increase results in a higher sublimation temperature. As the model's predicted sublimation temperature corresponds to the set far-field CO_2 concentration value, it tends to underestimate the measured values. Moreover, the predicted sublimation temperature inaccuracies for all CO_2 concentrations also originate from the theoretical expressions for diffusion coefficient (Eq. (1)) and thermal conductivity of the CO_2 and N_2 mixture (Eq. (11)), which are accurate upto approximately 8 % [24] and 2 % [23], respectively. To address these inaccuracies, a color-coded band around the model data for a given concentration level is illustrated in Fig. 8. The width of this band increases with decreasing CO_2 concentration, reflecting the larger magnitude of the diffusive component in Eq. (15), along with its associated error, for lower CO_2 concentrations.

All the measured and predicted data of the dry ice sublimation temperature as a function of far-field pressure and CO_2 concentration summarized in Fig. 8 is termed as the extended phase diagram of CO_2 consisting solid-vapor coexistence curves for various far-field concentration values.

An estimate of the dry ice sublimation temperature, when present in an unsaturated environment, is often made by evaluating the temperature from the standard phase diagram at the partial pressure of CO_2 in the ambient. By comparing this estimate with the measured data of the dry ice sublimation temperature for different far-field CO_2 concentrations, we show that this estimate can be erroneous. In Fig. 9, dry ice sublimation temperature is shown as a function of partial pressure. The steady-state values of the measured dry ice sublimation temperature for corresponding concentration values shown in Fig. 5 a) are taken, the concentration values are converted to the partial pressure of CO_2 using
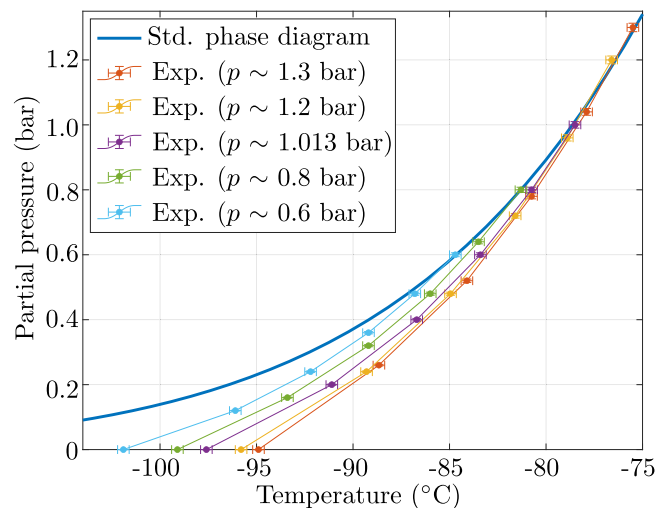

Fig. 8. This extended phase diagram illustrates the measured and predicted sublimation temperatures of dry ice (top and bottom x-axis) across a range of far-field pressures (y-axis) and CO_2 concentrations.

Fig. 9. Sublimation temperature of dry ice (x-axis) at different total pressure shown as a function of the partial pressure of CO_2 (y-axis) in the ambient.

ideal gas law, and these two data sets are plotted against each other for each far-field pressure to obtain the Fig. 9. This data is compared with the solid-vapor coexistence line from the phase diagram of CO_2. It can be seen from Fig. 9 that the agreement between the measured values and that of the phase diagram is good for points where the partial pressure of CO_2 is the same as the absolute pressure, i.e. for 100%vol concentration. For all the other data points, the measured sublimation temperature and the one estimated using partial pressure from the phase diagram are considerably different. The lower the concentration of CO_2 (or partial pressure), the larger is the difference from the phase diagram. Therefore, it is important to consider heat and mass transport phenomena in the surroundings of dry ice to evaluate its sublimation temperature instead of approximating its value at the partial pressure of CO_2 from the phase diagram of CO_2.

In this study, the objective is to evaluate the sublimation temperature of dry ice during its sublimation process in $N_2 - CO_2$ gas mixture. It is important to note that the typical use of dry ice involves sublimation in atmospheric air, and as a consequence, the transport properties, namely, diffusion coefficient and thermal conductivity may deviate from those observed in pure N_2 gas. The molecular diffusion coefficient of CO_2 in air at a specified temperature, denoted as T, and a pressure of 1 atm, is determined through the relationship proposed by Massman [27], given as $D(T, 1) = D(0, 1)(T/T_0)^{1.81}$. Here, $D(0, 1) = 13.81$ mm^2/s signifies the diffusion coefficient assessed at the reference temperature $T_0(0°C)$ and a pressure of 1 atm. By applying this equation, the diffusion coefficient of CO_2 in air at 20°C is computed to be 15.69 mm^2/s. Under similar conditions, the diffusion coefficient of CO_2 in N_2 gas is approximately 16 mm^2/s, as reported by Cussler [24]. Furthermore, the thermal conductivity of air and pure nitrogen gas does not exhibit substantial disparities. For instance, the thermal conductivity of air at a temperature of 300 Kelvin and a pressure of 1 bar is 26.4 mW/(m K), while the corresponding value for N_2 gas is 26.0 mW/(m K), as documented by NIST [28]. Based on the aforementioned analysis, it is evident that the transport properties of air and pure nitrogen gas maintain a negligible variance. Consequently, the findings elucidated in this paper hold potential relevance for diverse applications, up to the precision required for engineering activities.

5. Conclusion

An experimental and theoretical investigation into the influence of far-field CO_2 concentration and pressure on the sublimation of a dry ice sphere is described in this work. The experimental component involved measuring the sublimation temperature of two different sizes of dry ice spheres suspended in a controlled ambient environment composed of an $N_2 - CO_2$ gas mixture, encompassing a wide range of pressures and CO_2 concentrations. It was observed that the size of the dry ice did not influence its measured sublimation temperature when the dry ice was in thermal equilibrium with its surroundings at a given CO_2 concentration and pressure. The results presented in this paper demonstrate that, for a specific far-field pressure, the sublimation temperature of dry ice decreases as the far-field CO_2 concentration reduces due to sublimative cooling. This reduction leads to the attainment of a lower thermodynamic wet-bulb temperature, corresponding to a lower steady-state CO_2 concentration. At nearly 0%vol far-field CO_2 concentration and 1 atm pressure, the sublimation temperature decreases by 19 °C from the typical literature value of −78.5 °C for dry ice under saturated conditions. Furthermore, the far-field pressure of the surrounding environment where dry ice is undergoing sublimation also affects its sublimation temperature. Specifically, when the pressure in this environment decreases while keeping the far-field CO_2 concentration constant, the temperature at which dry ice sublimates also decreases. This effect is attributed to the fact that the diffusion coefficient of CO_2 vapor in the gaseous mixture increases as ambient pressure reduces, thereby enhancing sublimation from the dry ice surface and leading to cooling to

a lower sublimation temperature.

To graphically evaluate the sublimation temperature of dry ice, a mathematical model is developed that considers the heat and mass transport phenomenon, along with the temperature-dependent transport properties of the ambient gas. The predicted sublimation temperature values for a broad range of far-field pressures and CO_2 concentrations were found to agree well with the experimental values. Despite its simplicity and limitations, the findings presented in this study may prove useful in various industrial and scientific applications involving dry ice by accurately reflecting its sublimation temperature corresponding to the required far-field pressure and CO_2 concentration.

CRediT authorship contribution statement

A.S. Purandare: Conceptualization, Methodology, Data analysis, Experiments, Modeling, Writing; **W. M. Verbruggen**: Methodology, Data analysis, Experiments; **S. Vanapalli**: Conceptualization, Supervision, Review and editing, Project administration, Funding acquisition.

Declaration of Competing Interest

The authors declare no conflicts of interest.

Data availability

The data sets analyzed for this manuscript are available upon prior and reasonable request by contacting the corresponding authors.

Acknowledgments

References

[1] C. Rountree, C. Van Kirk, H. You, W. Ding, H.D. Van Guilde, W.M. Freeman, Clinical application for the preservation of phospho-proteins through in-situ tissue stabilization, Proteome Sci. 8 (2010) 61, https://doi.org/10.1186/1477-5956-8-61.

[2] C.J. Capicciotti, J.D.R. Kurach, T.R. Turner, R.S. Mancini, J.P. Acker, R.N. Ben, Spray cooling heat transfer: the state of the art, Sci. Rep. 11 (2015) 9692, https://doi.org/10.1038/srep09692.

[3] K. Byrnes, P. Washington, S. Knoblach, E. Hoffman, A.I. Faden, Delayed inflammatory mrna and protein expression after spinal cord injury, J. Neuroinflammation 8 (2011) 130, https://doi.org/10.1186/1742-2094-8-130.

[4] J.W. Ong, T. Minifie, E.S. Lin, H.A. Abid, O.W. Liew, T.W. Ng, Cryopreservation without dry ice-induced acidification during sample transport, Anal. Biochem. 608 (2020) 113906, https://doi.org/10.1016/j.ab.2020.113906.

[5] M. Jamil, N. He, X. Huang, W. Zhao, M.K. Gupta, A.M. Khan, Measurement of machining characteristics under novel dry ice blasting cooling assisted milling of aisi 52100 tool steel, Measurement 191 (2022), https://doi.org/10.1016/j.measurement.2022.110821.

[6] R. Sherman, Chapter 16 - carbon dioxide snow cleaning, in: R. Kohli, K. Mittal (Eds.), Developments in Surface Contamination and Cleaning, second edition, William Andrew Publishing, 2016, pp. 695–716, https://doi.org/10.1016/B978-0-323-29960-2.00016-2.

[7] B. Kochtubajda, E.P. Lozowski, The sublimation of dry ice pellets used for cloud seeding, J. Clim. Appl. Meteorol. 24 (1985) 597–605, https://doi.org/10.1175/1520-0450(1985)024<0597:TSODIP>2.0.CO;2.

[8] G.G. Wells, R. Ledesma-Aguilar, G. McHale, K. Sefiane, A sublimation heat engine, Nat. Commun. 6 (2015) 6390, https://doi.org/10.1038/ncomms7390.

[9] L. Chen, X. Zhang, A review study of solid-gas sublimation flow for refrigeration: from basic mechanism to applications, Int. J. Refrig. 40 (2014) 61–83, https://doi.org/10.1016/j.ijrefrig.2013.11.015.

[10] D. Quéré, Leidenfrost dynamics, Annu. Rev. Fluid Mech. 45 (2013) 197–215, https://doi.org/10.1146/annurev-fluid-011212-140709.

[11] G. Dupeux, T. Baier, V. Bacot, S. Hardt, C. Clanet, D. Quéré, Self-propelling uneven leidenfrost solids, Phys. Fluids 25 (2013), 051704, https://doi.org/10.1063/1.4807007.

[12] M. Shi, X. Ji, S. Feng, Q. Yang, T.J. Lu, F. Xu, Self-propelled hovercraft based on cold leidenfrost phenomenon, Sci. Rep. 6 (2016) 1–7, https://doi.org/10.1038/srep28574.

[13] M. Shi, F. Frank, L. Wang, F. Xu, T.J. Lu, C.P. Grigoropoulos, Role of jakob number in leidenfrost phenomena unveiled by theoretical modeling, Phys. Fluids 31 (2019) 4, https://doi.org/10.1063/1.5082266.

[14] A. Parrenin, R.W. Liefferink, D. Bonn, Dry ice hoverboard: Friction reduction by the leidenfrost effect, Phys. Rev. E 103 (2021), https://doi.org/10.1103/PhysRevE.103.023002.

[15] M.R.O. Panão, J.J. Costa, M.R.F. Bernardo, Thermal assessment of sublimation cooling with dry-ice sprays, Int. J. Heat Mass Transf. 118 (2018) 518–526, https://doi.org/10.1016/j.ijheatmasstransfer.2017.11.015.

[16] W. Wang, J. Niu, Y. Li, K. Ren, Numerical study on heat transfer enhancement by spray-sublimation cooling with dry ice particles, Int. J. Multiphase Flow 214 (2022), https://doi.org/10.1016/j.applthermaleng.2022.118809.

[17] S. Kwak, J. Lee, Eulerian multiphase analysis for heat transfer enhancement by co 2 sublimation in slot jet impingement, Int. J. Multiphase Flow 107 (2018) 182–191, https://doi.org/10.1016/j.ijmultiphaseflow.2018.05.024.

[18] K. Sefiane, S.K. Wilson, S. David, G.J. Dunn, B.R. Duffy, On the effect of the atmosphere on the evaporation of sessile droplets of water, Phys. Fluids 21 (2009), https://doi.org/10.1063/1.3131062.

[19] X. Xu, L. Ma, Analysis of the effects of evaporative cooling on the evaporation of liquid droplets using a combined field approach, Sci. Rep. 5 (2015), https://doi.org/10.1038/srep08614.

[20] N. Fukuta, W.A. Schmeling, Experimental determination of ice nucleation by falling dry ice pellets, J. Clim. Appl. Meteorol. 10 (1971), https://doi.org/10.1175/1520-0450(1971)010<1174:EDOINB>2.0.CO;2.

[21] CO2METER.COM, GSS Sensor User's Manual: COZIR, SprintIR, MISIR and MinIR Sensors, Rrevi edition, August 2015.

[22] MKS Instruments, Six Shattuck Road Andover, MA 01810–2449, MKS Baratron Type 622A/626A/627A/628A/629A Absolute Pressure Transducers, 114492nd Edition, 2023.

[23] E.W. Lemmon, I.H. Bell, M.L. Huber, M.O. McLinden, NIST Standard Reference Database 23: Reference Fluid Thermodynamic and Transport Properties-REFPROP, Version 10.0, National Institute of Standards and Technology, 2018, https://doi.org/10.18434/T4/1502528. URL, https://www.nist.gov/srd/refprop.

[24] E.L. Cussler, Diffusion Mass Transfer in Fluid Systems, 3rd Edition, Cambridge University Press, The Edinburgh Building, Cambridge CB2 8RU, UK, 2009.

[25] J.H. Lienhard IV, J.H. Lienhard V, A Heat Transfer Textbook, 3rd edition, Phlogiston Press, Cambridge, Massachusetts, U.S.A, 2003.

[26] J.P. Holman, Thermodynamics, 4th edition, McGraw-Hill, New York, 1988.

[27] W.J. Massman, A review of the molecular diffusivities of H_2O, CO_2, CH_4, CO, O_3, SO_2, NH_3, N_2O, NO, and NO_2 in air, O_2 and N_2 near stp, Atmos. Environ. 32 (1998), https://doi.org/10.1016/S1352-2310(97)00391-9.

[28] M.L. Huber, A.H. Harvey, Thermal Conductivity of Gases, URL, https://tsapps.nist.gov/publication/get_pdf.cfm?pub_id=907540.